SLAC-PUB-3140
June 1983
(I)

THE BARREL SHOWER COUNTER FOR THE MARK III DETECTOR AT SPEAR*

Walter Toki[1], Kirk Bunnell[1], Ronald Cassell[2], Knut Skarpaas[1], Jeffery Becker[2], John Brown[4], Kevin Einsweiler[1], James Russell[3], Anthony Spadafora[2], Hans-Juergen Willutzki[4], William Wisniewski[2]

ABSTRACT

The barrel shower counter used in the Mark III detector at SPEAR is described. This unimodular cylindrical detector is placed inside the Mark III solenoidal magnet coil. The design, construction details and electronics are discussed. Its performance is studied using high statistics data from $\psi(3095)$ decays. The main features are 76% of 4π sr solid angle coverage, good detection efficiency for photons down to 100 MeV, fine segmentation to obtain 7 mr angular resolution in the azimuthal angle ϕ, position resolution of 0.8% x wire length in the axial direction using charge division and overall energy resolution of $17.5\%/\sqrt{E}$.

Submitted to Nuclear Instruments and Methods

---

* Work supported by the Department of Energy, contract DE-AC03-76SF00515.
[1] Stanford Linear Accelerator Center, Stanford, CA 94305, U.S.A.
[2] University of Illinois at Urbana-Champaign, Urbana, IL 61801, U.S.A.
[3] California Institute of Technology, Pasadena, CA 91125, U.S.A.
[4] University of Washington, Seattle, WA 98195, U.S.A.

A. INTRODUCTION

The Mark III barrel shower detector features good position and energy resolution, large solid angle coverage and good photon detection efficiency at moderate cost. In particular, good detection efficiency for low energy photons and large solid angle coverage were given a high priority. This requirement for low energy photon coverage necessitated putting the barrel shower detector inside the magnet coil. The desire for excellent solid angle coverage with a minimum of "cracks" and the need to allow ample room radially inside for a sizable drift chamber required a unimodular cylindrical design. To keep the cost acceptable and still have adequate position and energy resolution a finely segmented proportional resistive wire chamber interspersed with 0.5 radiation length lead panels was used. The detector described here was built at SLAC during 1980 and installed in the West pit at SPEAR in August, 1981. The detector performance was analyzed on data logged in the spring of 1982. The barrel shower counter is augmented by end cap shower counters which are similar in concept to the barrel and described in detail elsewhere.[1]

B. MECHANICAL DESIGN AND CONSTRUCTION

1. Inner Spool

The requirement that the shower counter be cylindrical and unimodular called for the difficult design of a cylindrical inner spool which when supported solely at the ends could support the entire weight (≃29,000 kg) of the counter. The spool is made of aluminum of length 3.85 meters, outer diameter 2.52 m and thickness 23 +/- 4 mm. The variation in radius

over the entire outer surface is less than 1 mm. At both ends of the spool are flanges of length 83 mm extending radially outward an additional 51 mm. Through these flanges are 24 holes where outward radial stainless steel rods of 28.5 mm diameter support the detector inside the magnet. During the construction stage an internal "spider" structure supported the spool and was itself mounted on a frame which allowed the spool to be rotated. The ability to easily rotate the spool greatly facilitated the assembly of the lead panels and the stringing of the wires. The outer surface of the spool itself serves as the inner boundary for the first radial layer of proportional wire cells.

2. Lead Panel Structure and Construction

In order to achieve good energy resolution it was decided to have 24 radial layers of sampling interspersed with 23 layers of 0.5 radiation length lead. The aluminum spool and time of flight scintillation counters account for approximately 0.4 radiation lengths of material before the first sampling layer. Monte Carlo studies and prototype beam tests indicated it was of minimal advantage to vary the thickness of the absorber in different layers. The cylindrical structure required the lead layers also be cylindrical and of 23 different radii. To accomplish this and provide structural strength for the lead sheets, cylindrical panel sandwiches made up of aluminum clad lead were built. There are 10 such panels per layer. The panel widths vary from 0.798 m for the innermost layer to 1.038 m for the outermost layer. The length of the panels is 3.48 m and uniform for all layers. The sandwiches consist of 0.64 mm Al interspersed with a layer of 0.25 mm film adhesive on each

side of the 2.8 mm Pb sheets. In addition the lead was alloyed with 6% antimony for increased stability.

The panel construction process consisted of adjusting a curved table to the required curvature for a particular layer. The sandwiches were made by stacking the Al-glue-Pb-glue-Al on to the table. Then finally a polypropolene sheet sealed around the perimeter provided a vacuum bag to consolidate and compress the layers against the curved table. The entire table with the sandwich layup was then put into an oven (150° C) and cured for two hours while under "vacuum pressure". The finished curved panels were then transferred to a large milling machine where, still clamped to their exact curvature by "vacuum pressure", they were trimmed to the correct size. To allow for accumulated errors, there was a "crack" of approximately 3.2 mm allowed between panels. This "crack" was rotated in azimuthal position for each layer such that it never was located at the same azimuthal angle (ϕ) for any of the layers. Figure 1 shows a diagram of the assembly.

3. Cell Structure and Construction

In order to have adequate position resolution there are 320 cells per radial layer making a total of 7680 cells. The cells, centered on a stainless steel wire are bounded by the aluminum from the Al-Pb-Al sandwiches on the two radial sides and by I-beams on the circumferential sides. The I-beams are aluminum extrusions of width 10.0 mm, radial height 12.4 mm and thickness 0.76 mm. The wire (Stablohm 800) is 46 microns in diameter, 3.48 m in length for each cell and has a resistance $\simeq$ 2600 ohms. The radial height of the cells is 12.5 mm and the width

varies from 24.1 mm for the innermost layer cell to 32.2 mm for the outermost layer cell. The height of the cells is fixed by aluminum ribs running circumferentially and also by the I-beams. The ribs are aluminum extrusions and there are 5 ribs per panel evenly spaced apart axially. The ribs are 12.5 mm in radial height and 26.7 mm in axial length. Along the top of the ribs there is a groove 13.4 mm wide and 1.9 mm deep. In this groove two layers of stainless steel straps (12.7 mm wide and 0.64 mm thick) were wound under tension forming bands which provide the sole support holding a completed layer together. Since the ribs carry the load of the lead panels, it was very important that they be on top of each other in successive radial layers. The presence of the ribs creates a dead area of approximately 50 mm in the axial direction (z) for each of the 3 inner ribs. See Fig. 6 for a plot showing the effect of these ribs on the acceptance .

These ribs have precisely predrilled holes for locating the wires. In each hole a plastic (General Electric VALOX 310) feed-through in the shape of a funnel is secured. These feed-throughs locate the wires in space, insulate the wire from the aluminum ground, facilitate stringing the wires and provide a gas manifold for the dispersal of gas throughout the chamber. The feed-throughs have a cylindrical part of OD = 6.2 mm and an ID = 1.6 mm. At one end the feed-through flares out at an angle of 60^0 into a rectangular cross section which fills the cell boundary between the panels and the I-beams. The I-beams are held in place between the ribs by compression between the feed-throughs at one end and phosphor-bronze clips which fit around the cylindrical portion of the feed-throughs at the other end.

In the initial phase of the construction process the ribs, with the precision holes already drilled in them, were annealed and rolled to the proper radius for a given layer. The outer rectangular flange of the funnel section of feed-throughs was cut to the appropriate width for a layer (5x320=1600 per layer). The outer feed-throughs (those in the outer two ribs of each panel) had a small (1.5 mm) hole punched in the flange part as a gas feed for each cell. The I-beams were also cut to the proper length for each layer. This length varies because the flared feed-through flange which holds the I-beams at one end has a different length for each layer as well as a different width. In addition, the clips to hold the I-beams in place also were cut to the proper width for each layer. The ribs, I-beams, feed-throughs and clips were all chemically cleaned.

Following this, all the components were moved into a clean room. The outer feed-throughs were then epoxied in the holes in the outer ribs. The five ribs per panel were then precisely located on the panels and anchored by means of stainless steel bolts. The other feed-throughs for the inner three ribs were put in place and the clips and most of the I-beams were then installed. A set of ten identical panels for one layer were then mounted on the cylinder and held temporarily by means of clamps. After careful alignment of each panel (to within 0.5 mm) a stainless steel strap was wound around each of the five rib locations. A layer of Teflon tape had previously been put in the rib grooves to provide a low friction surface for the straps. The straps were then pulled to 600 lbs. tension using a specially made pneumatic tool. While under tension each of the straps was spot welded to itself to form a

band. A second layer of Teflon tape was then added on top of each of the now banded straps and a second layer of strap was added and similarly tensioned and spot welded.

The stainless steel wires were now strung for an entire layer. The stringing procedure was to pass a rotating narrow rod through the feed-throughs of a cell. The rod was offset in such a way that as it was rotated and advanced it would locate the funnel. After the rod was all the way through a set of five feed-throughs it was retracted with the wire attached to it thus stringing the wire. At both ends the wire was then passed through small (1.6 mm OD , 0.4 mm ID) cylindrical stainless steel pins that were press fitted into the outer feed-throughs. The wire was tensioned to 90 gms and the pins crimped. At the completion of each layer the wires were tested for resistance and also tension by passing oscillating current through each of them and measuring its resonance in the field of a small bar magnet. Wires away from nominal value of resistance or tension by more than 10% were replaced. A virtue of this stringing procedure was that it could be used to replace broken wires even after completion of the entire detector.

The only exceptions to this overall assembly method were the innermost layer where the ribs were mounted directly to the outer spool surface, and the outermost layer where the outer panels were simple Al-Al sandwiches instead of Al-Pb-Al. At the conclusion of the construction, the entire outer radial surface was wrapped with fiberglass epoxy to make a good gas seal. At the ends the cracks between the panels and the ribs

were sealed using a layer of Dow Corning Silicone Rubber and then a sprayed coat of General Electric Glyptal.

4. Cooling

The entire detector is supported by the stainless steel straps under tension. This tension would be reduced if ,for example, the lead plates should creep. Since creep is a strong function of temperature, an equivalent arrangement of Al-Pb-Al sandwiches was tested under pressure at different temperatures. It was found that the creep would be tolerable at temperatures below 32^0 C. To ensure that the temperature would remain below this by thermally insulating the detector from the magnet coil, the primary heat source, water cooled copper jackets were manufactured and inserted in the 25 mm radial space between the shower counter and the coil. Thermocouples were also placed on the barrel and monitored routinely during data runs.

C. GAS

The gas mixture used in the system is 80% Argon/ 20% Methane. Gas flow through the detector is at the rate of one volume exchange per day ($\simeq$ 425 liters/hour). The gas is not recirculated but simply passed out into the atmosphere. While some small leaks are unavoidable in a large system such as this, gas leaving the chamber at this flow has less than 500 ppm of oxygen compared with an input purity $\simeq$ 25 ppm of oxygen. This amount of air leaking into the chamber results in a gain loss of several percent. Gain monitoring is done on line as well as atmospheric pressure and temperature monitoring for later corrections. In addition, each

shipment of gas is carefully analyzed to check the gain variation. If the gain of the gas is too high the high voltage must be reduced accordingly to avoid charge pile up.

D. ELECTRONICS

In order to achieve maximum efficiency and resolution for low energy photons, every wire for the first six layers is read out individually from both ends. In subsequent layers, the wires are ganged in groups of three radially. The signals from each end of a wire (or a triplet of wires) is read out and stored in sample-and-hold circuits (ISHAMs, Integrated Amplifier and Sample-and-Hold Analog Multiplexers, see Ref. 2 and Fig. 2). The ISHAM electronics is packaged 24 channels to a card and 20 cards to a crate. The cards and crates are both specially designed for the shower counter electronics. The crates are placed near each end of the detector (8 per end) to shorten the signal cable length (4.3 m) and to reduce cable noise and cable costs. The total electronic and cable noise for a 1 microsecond gate is 5 femtocoulombs. The minimum ionizing charge deposit per cell is 1 picocoulomb which yields a S/N ratio of 200. The cables (custom made RG-174 Belden 50 ohm coax) supply the high voltage from the boards to the wires. The high voltage is isolated from the electronics by a 25 nF/3 kV capacitor mounted on the boards. Before installation of the cables to the ISHAM boards, the cables were tested in place on the chamber. This was done by filling the chamber with nitrogen gas and setting the high voltage to 3 kV. The cables were individually checked for current leakage and bad ones were replaced. The bad ones (<0.5%) were all a result of bad crimps at the

cable ends. The sense wires are nominally run at 2100 volts during data taking giving a gain of approximately 5 x 10^4 .

The ISHAM circuitry (Fig. 2) consists of an amplifier followed by a sampling gate and a sample-and-hold unit. Following this, the output is sent at the command of a trigger signal via a CAMAC controlled multiplexer to a BADC (Brilliant ADC)[3]. At the BADC the signal is compared with a threshold, pedestal subtracted and corrected for gain variations (including a quadratic term). The BADC output is transmitted digitally to the VAX data logging computer. To correct for variations in gain for each electronic channel, the units are calibrated on the average of once per day. The calibration procedure consists of putting a fixed charge on the amplifier input and determining the values of the threshold, pedestal, linear gain and quadratic term in the BADCs.

E. PERFORMANCE

Two sample events from the one event display are shown in Figs. 3 and 4. Figure 3 shows a Bhabha scattering event $e^+e^- \Longrightarrow e^+e^-$ at ECM = 3.095 GeV. In this figure the axial and transverse views are each shown. Figure 4 shows the axial view of the decay $\psi(3095) \Longrightarrow \pi^+ \pi^- \gamma \gamma \gamma$. The measured energy of each of the photons is indicated on the figure.

A detailed study has been made of the photon detection efficiency. Of particular interest is the efficiency for low energy photons. To study the efficiency as a function of photon energy, the final state $\psi(3095) \Longrightarrow \pi^+ \pi^- \pi^0$ was used. Using the drift chamber to determine the momenta of the two charged pions, the momentum of the π^0 was determined. Then,

using the π^0 momentum and detecting one photon from its decay and therefore knowing its position and angle, the position and angle of the second photon could be predicted. The efficiency at a given photon energy was determined as the ratio of the number of found photons divided by the total number of predicted photons at the same energy. The results are shown in Fig. 5. As can be seen the efficiency is very good down to 100 MeV where it falls to ≈75%. This method is not without a small uncertainty, however, since two approximately equal energy photons could be confused with a single high energy photon combined with a very low energy one. This results when the two equal energy photons having small angular separation are separated only in θ (or z) but not in ϕ.

Position and therefore angular resolution is ultimately limited by the cell size in the ϕ coordinate and the charge division resolution on the z axis. Figure 6 shows a plot of the energy of Bhabha scattered electrons versus z position from charge division. The presence of the ribs is clearly seen in the plot at z=0.0, +/-0.8 m, and +/-1.6 m. While obviously causing some inefficiency, the ribs do serve as a calibration tool. The z position resolution obtained using cosmic ray events and back to back muons is 0.8% x wire length as shown in Fig. 7. There is a ϕ angular segmentation of $2\pi/320 \simeq 20$ mr due to the cell size since there are 320 cells per layer. The ϕ angle for a shower is determined by using the shower spread to reconstruct a shower origin. Using cosmic rays, muons and Bhabha scattered electrons the ϕ angular resolution was determined to be 7 mr as shown in Fig. 8.

The energy resolution and energy scale variations have been determined by using Bhabha events and also from energy constrained π^0 photons. In the latter case, locating one photon predicts the energy and direction of the other. In such determinations as well as all other data, corrections are made for atmospheric pressure and temperature variations as well as the losses due to the presence of the ribs. Using the above constrained photon technique, the variation of the energy scale has been investigated. Figure 9 shows the distribution of measured photon energy versus predicted energy. The data is seen to scale quite well down to 50 MeV. For the energy resolution determination, Figure 10 shows a plot of the energy spread at the ψ (3095) for Bhabha scattered electron events. This data and similar data at two other CM energies are shown in Fig. 11. This data is well fit by an energy resolution of $17.5\%/\sqrt{E}$.

The results of position and angular resolution, detection efficiency and energy resolution are easily seen in the ability of the detector to find particles that decay into photons. Figure 12 shows a plot of the invariant mass of two photons from events satisfying a constrained fit to the reaction $\psi(3095) \Longrightarrow \pi^+ \pi^- \gamma \gamma \gamma$. The π^0 peak is obvious as well as an η peak. The ability to resolve photons so cleanly is, of course, very valuable in the full reconstruction of events and also in the study of radiative decays. The mass resolution of the π^0s is 75 MeV FWHM as determined from π^0s in the reaction $\psi(3095) \Longrightarrow \pi^+ \pi^- \pi^0$.

F. SUMMARY

We have built a cylindrical unimodular shower counter with 24 radial sampling layers sandwiched between 23 layers of 0.5 radiation length

lead. The cylindrical geometry enabled the counter to be placed inside the magnet coil of the Mark III detector at SPEAR. The detector has been in operation since fall of 1981 and using the data accumulated we have determined the following properties of the shower counter; excellent photon detection efficiency as a function of energy extending down to ≃75% at 100 MeV, good position resolution of 0.8% x wire length using charge division in the axial direction, angular resolution of 7 mr in ϕ, energy resolution of $17.5\%/\sqrt{E}$ and good separation of photons allowing the clean determination of particles decaying into photons. The barrel shower counter described here covers 76% of 4π sr solid angle. When combined with the endcap shower counters[1] the overall coverage is 94% of 4π sr.

ACKNOWLEDGEMENTS

We gratefully acknowledge the help from W. Wadley in the construction of the detector, D. Bernstein, J. Bernstein and D. Hutchinson in the design and construction of the electronics, R. Fabrizio, H. Sadrozinski and the shops at UC Santa Cruz in the fabrication and checkout of the electronics and D. Hitlin, A. Odian, R. Mozley, T. Schalk and F. Villa for valuable discussions. We would like also to thank the staff of SLAC for assistance and technical support and the many people in the shops who contributed efforts of the highest quality. We also acknowledge the valuable assistance from H. Guldenmann and the shops at the University of Washington.

REFERENCES

1. R. Fabrizio et al. , to be published.

2. D. Bernstein and D. Hutchinson, IEEE Trans. Nucl. Sci. NS-29 No 1 (1982) 294.

3. M. Breidenbach et al., IEEE Trans. Nucl. Sci. NS-25 No 1 (1978) 706-710.

FIGURE CAPTIONS

1. Isometric view of the shower counter for the first seven layers. Representative view only, not to scale.

2. ISHAM electronics block schematic.

3. One event display of an event $e^+e^- \Longrightarrow e^+e^-$ (Bhabha scattering), ECM = 3.095 GeV, axial and transverse views. Hits are displayed (going radially outward) in the drift chamber, the time of flight counters and the barrel shower counter.

4. One event axial display of an event $\psi(3095) \Longrightarrow \pi^+ \pi^- \gamma \gamma \gamma$. P = track momenta in GeV as measured by the drift chamber, E = track energy in GeV deposited in the shower counter. (Track #1 goes into the endcap shower counter.)

5. γ Efficiency vs. γ Energy. (See text for details.)

6. Single track energy vs. z using Bhabha scattered electron events.

7. Z position resolution as determined by plotting the difference in the z measurement from the two tracks in muon pair and cosmic ray events. σ = 44 mm. The resolution σ/wire length = 0.8% after taking into account the vertex slewing in z of 18 mm and the factor of $\sqrt{2}$ because the difference in the two z measurements is used.

8. ϕ resolution using Bhabha and muon pair events and the central drift chamber to predict the position in the shower counter. σ = 7.3 mr. Overall resolution $\simeq$ 7 mr after taking into account the drift chamber error of $\sigma \simeq$ 2.5 mr.

9. Measured γ energy (y) vs. predicted γ energy (x). (See text for details.)

10. Energy of Bhabha scattered electrons at ECM = 3.095 GeV. σ = 0.217 GeV ==> $17.5\%/\sqrt{E}$ resolution.

11. Measured energy of Bhabha scattered electrons for three different beam energies. Data is shown for two different regions of cos θ.

12. $\gamma\gamma$ invariant mass for events satisfying a constrained fit to the hypothesis $\psi(3095)$ ==> $\pi^+ \pi^- \gamma \gamma \gamma$.

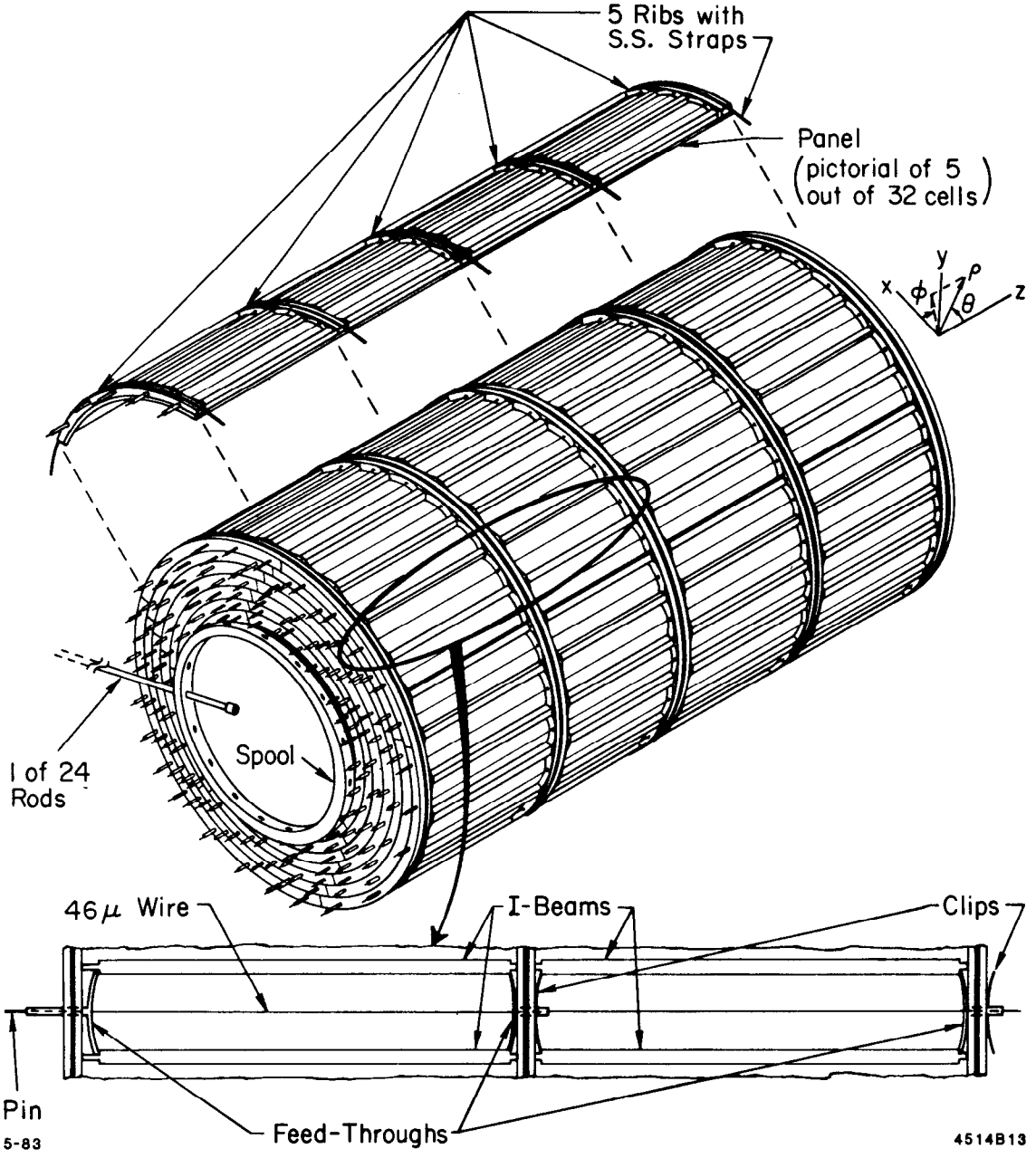
5 Ribs with
S.S. Straps
Panel
(pictorial of 5
out of 32 cells)
y
x
z
ρ
θ
1 of 24
Rods
Spool
46μ Wire
I-Beams
Clips
Pin
Feed-Throughs
5-83
4514B13

Fig. 1

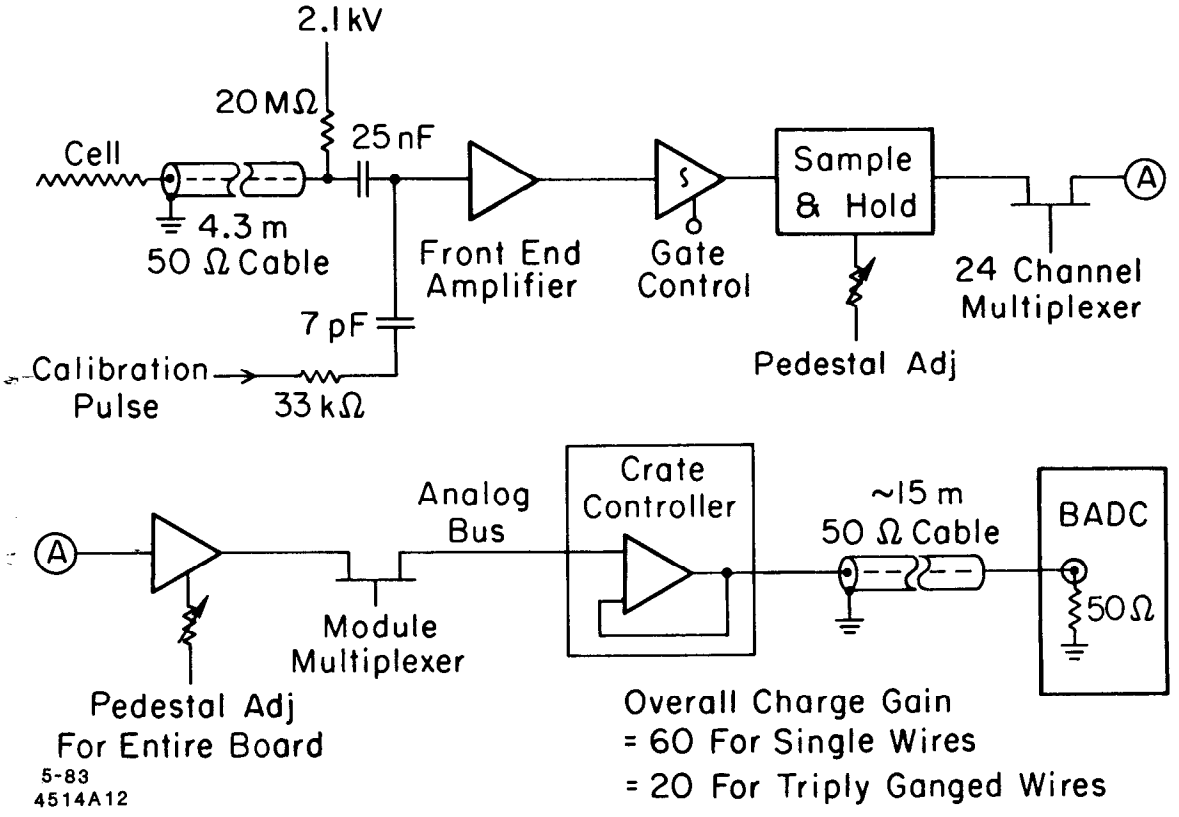
2.1 kV
20 MΩ
25 nF
Cell
4.3 m
50 Ω Cable
Front End
Amplifier
Gate
Control
Sample
& Hold
A
24 Channel
Multiplexer
7 pF
Calibration
Pulse
33 kΩ
Pedestal Adj
A
Analog
Bus
Crate
Controller
~15 m
50 Ω Cable
BADC
50 Ω
Module
Multiplexer
Pedestal Adj
For Entire Board
5-83
4514A12
Overall Charge Gain
= 60 For Single Wires
= 20 For Triply Ganged Wires

Fig. 2

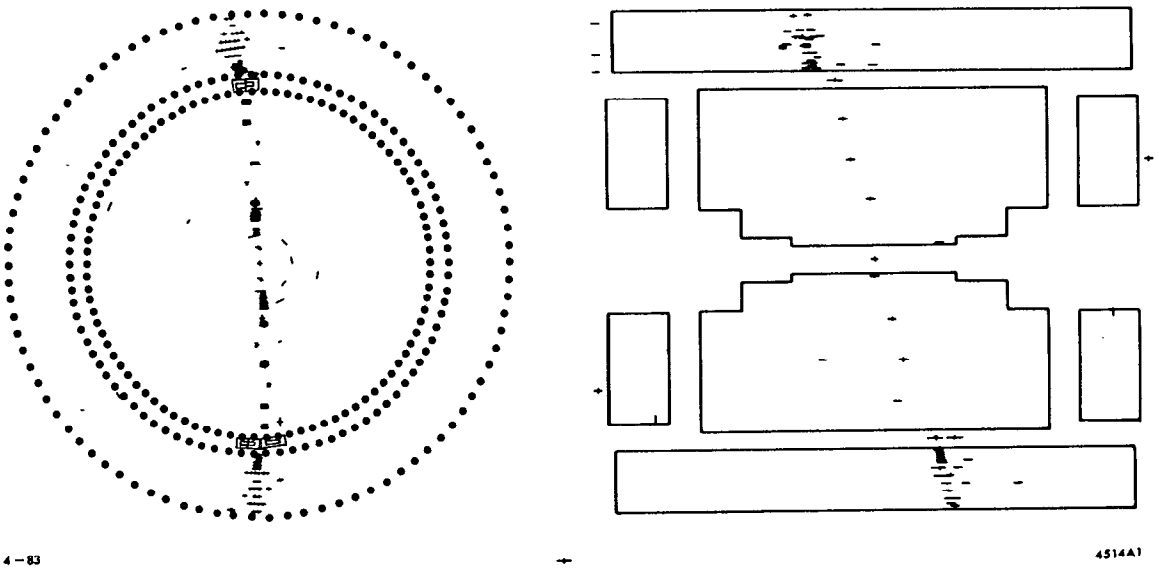

Fig. 3

N	P	E
1	0.39	0.16
2	0.44	0.19
3	0.0	1.77
4	0.0	0.49
5	0.0	0.13

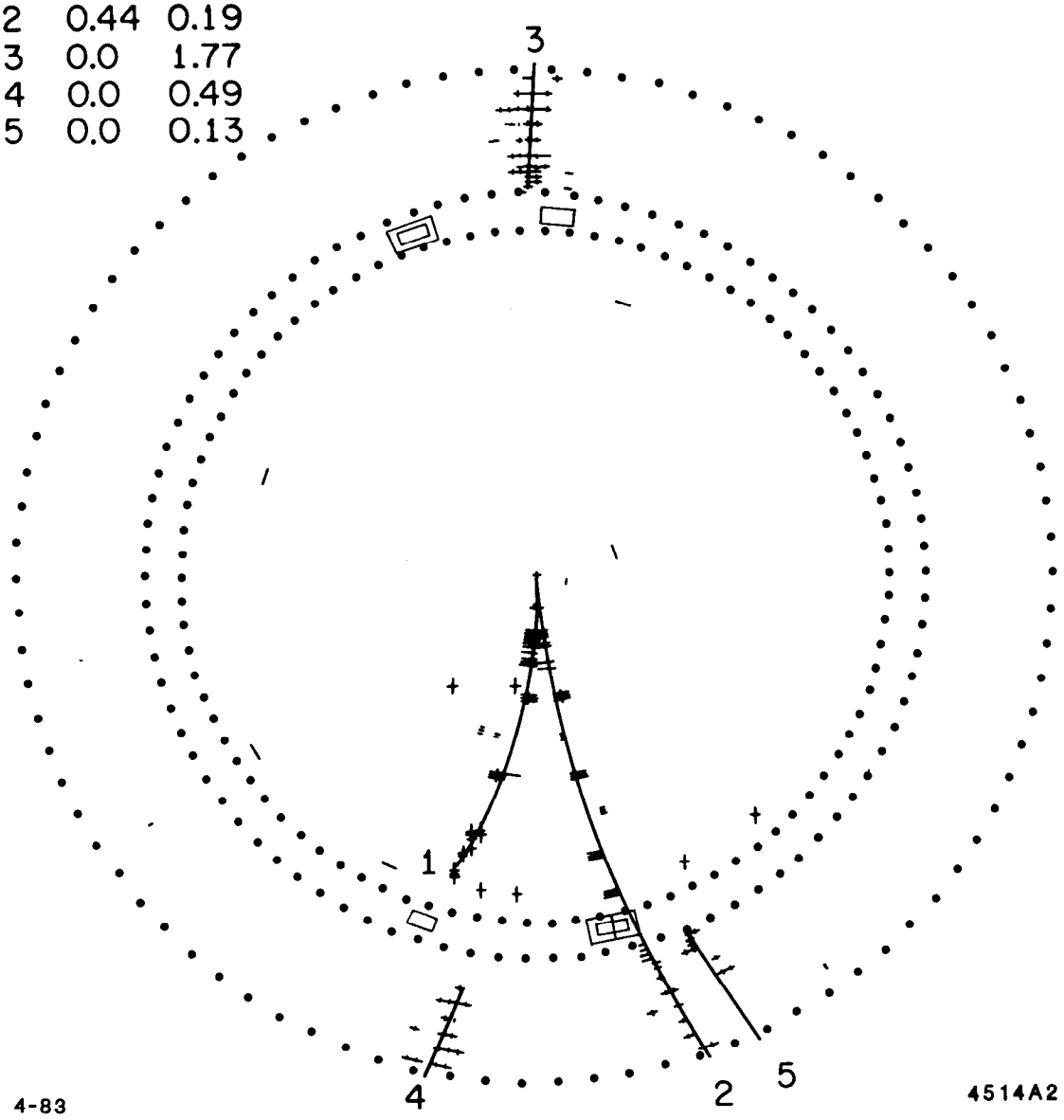

Fig. 4

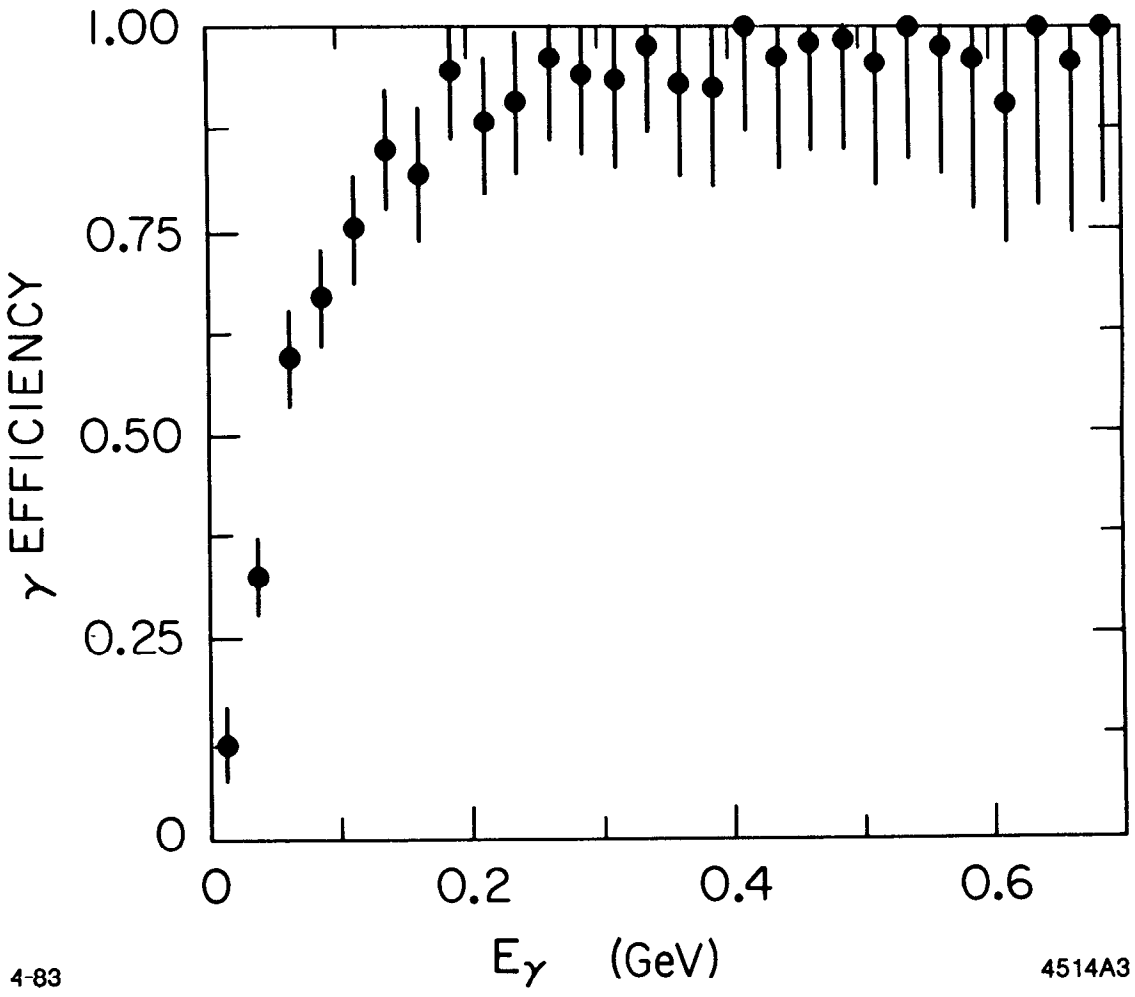

Fig. 5

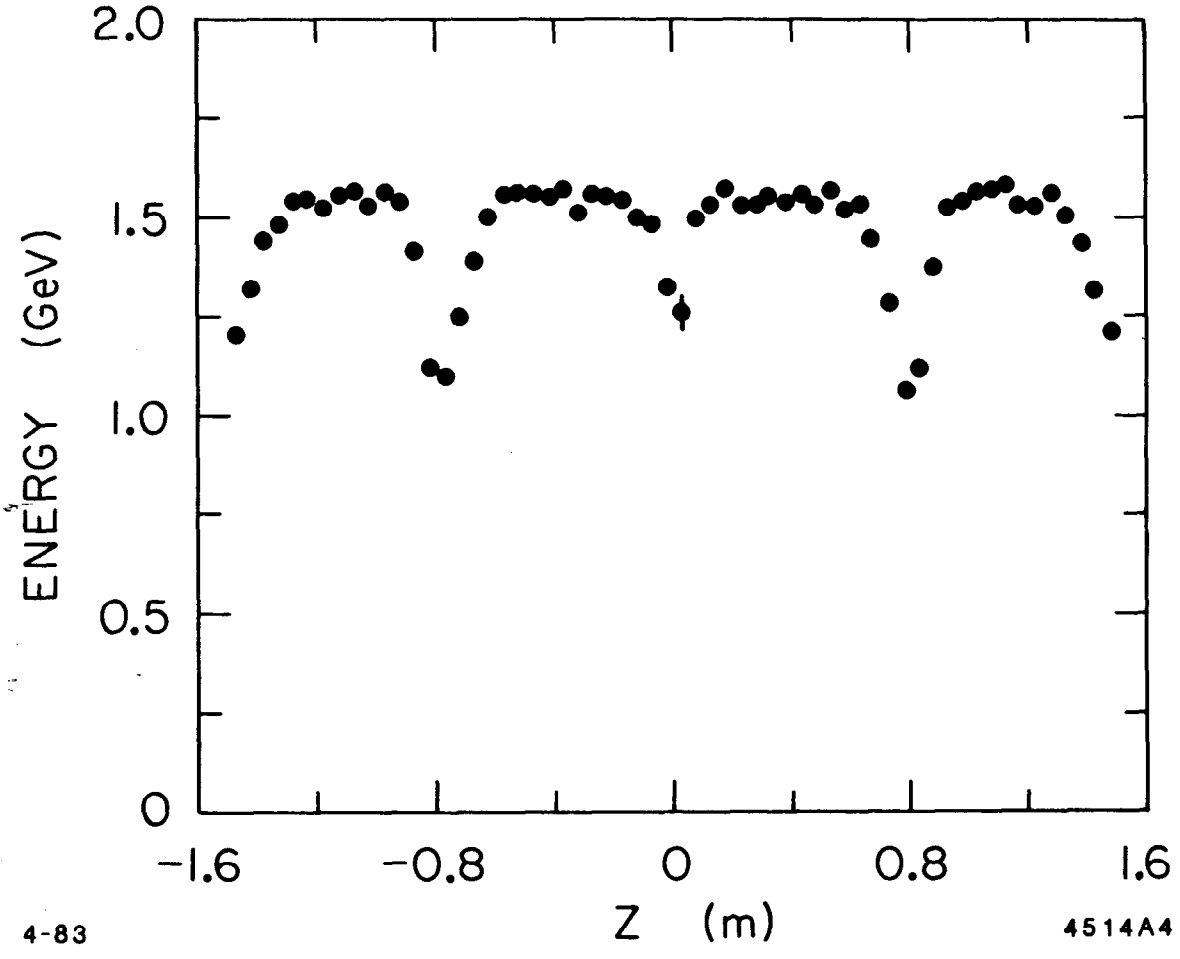

Fig. 6

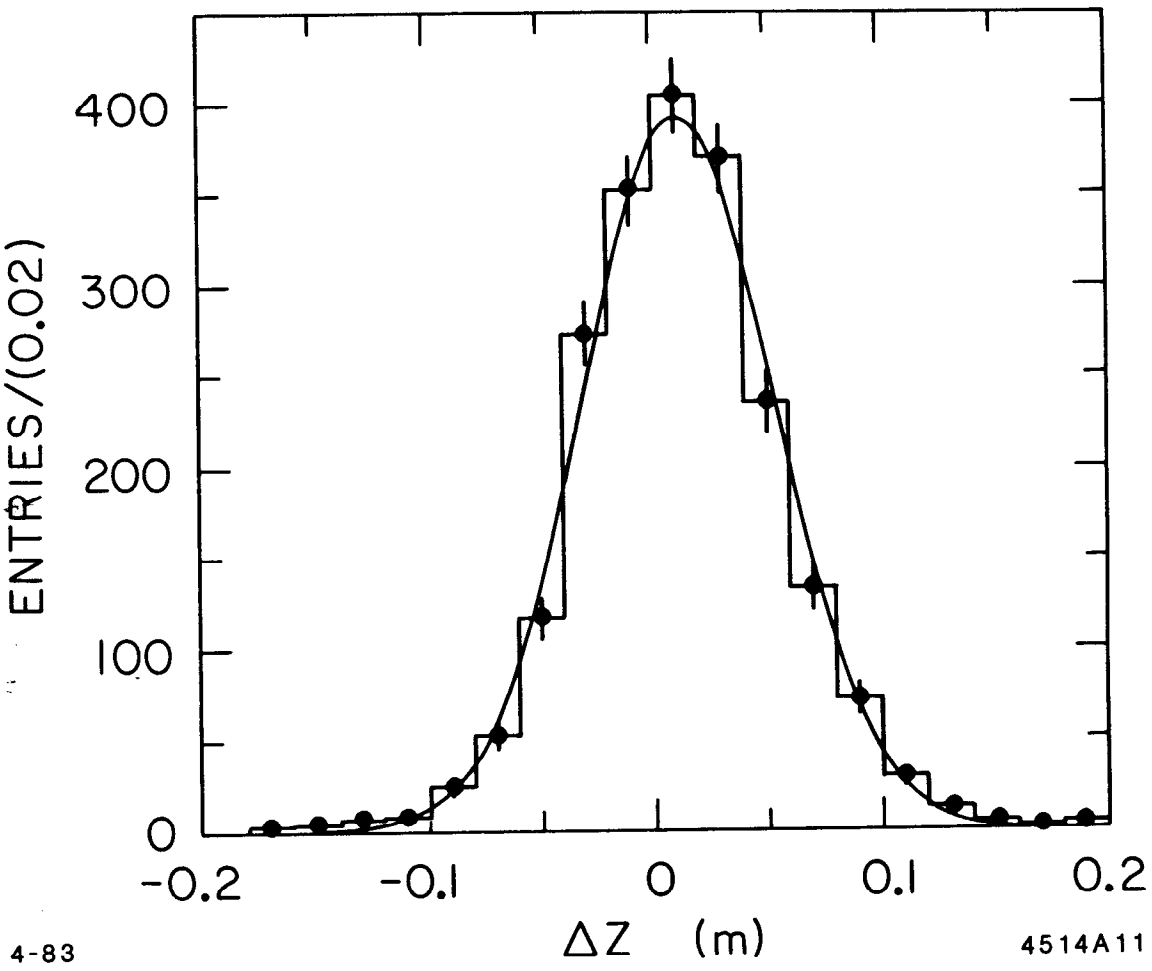

Fig. 7

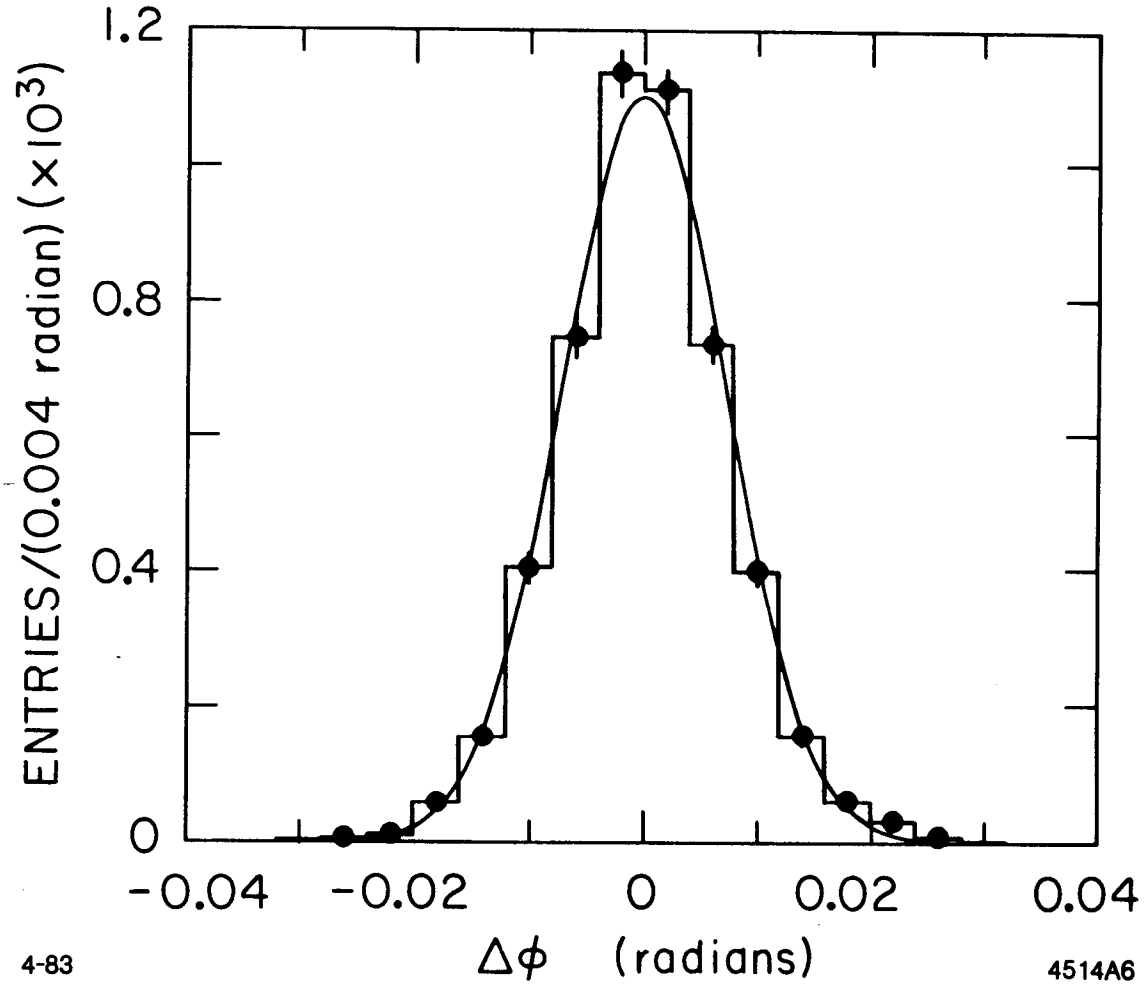
1.2
0.8
0.4
0
ENTRIES/(0.004 radian) (×10³)
-0.04
-0.02
0
0.02
0.04
Δφ (radians)
4-83
4514A6

Fig. 8

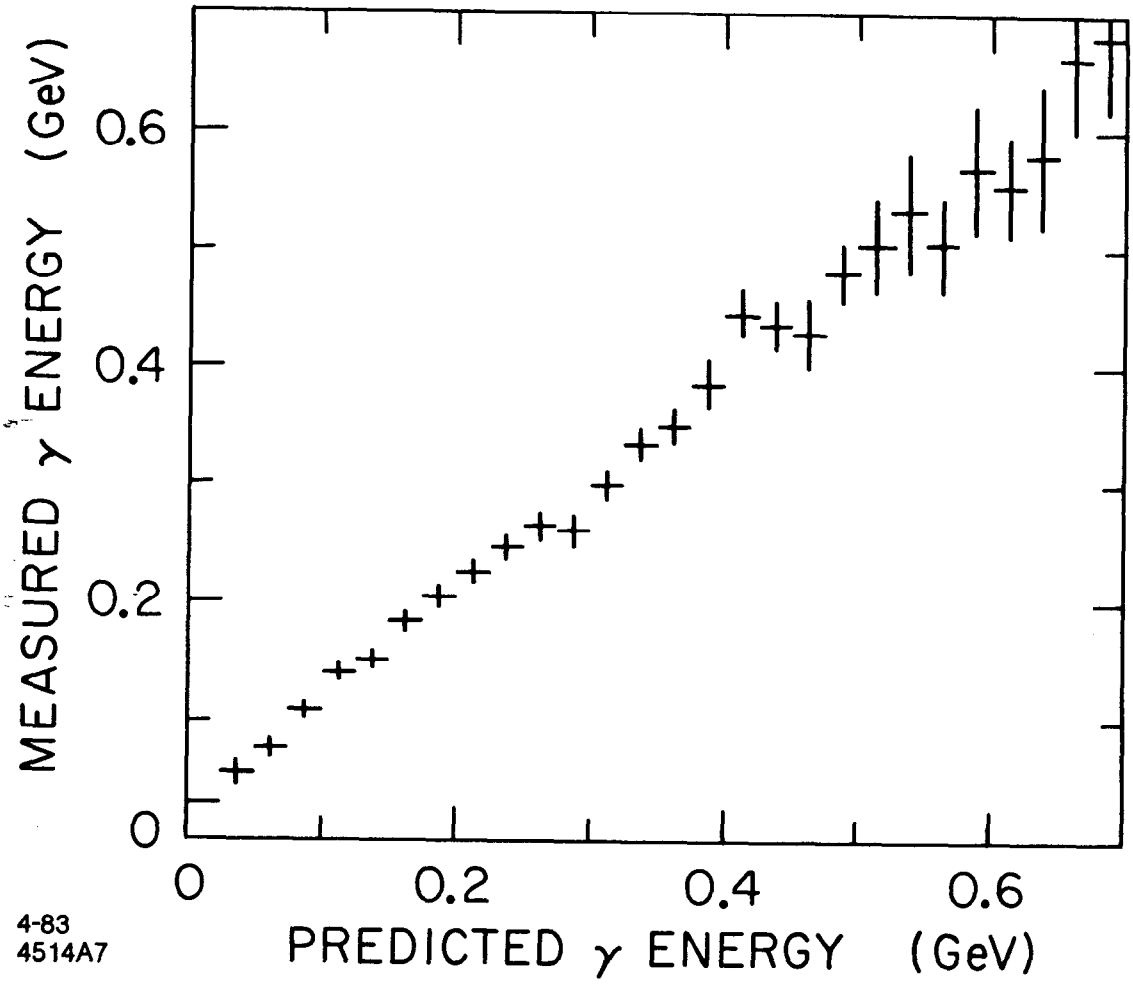
MEASURED γ ENERGY (GeV)
0.6
0.4
0.2
0
0
0.2
0.4
0.6
PREDICTED γ ENERGY (GeV)
4-83
4514A7

Fig. 9

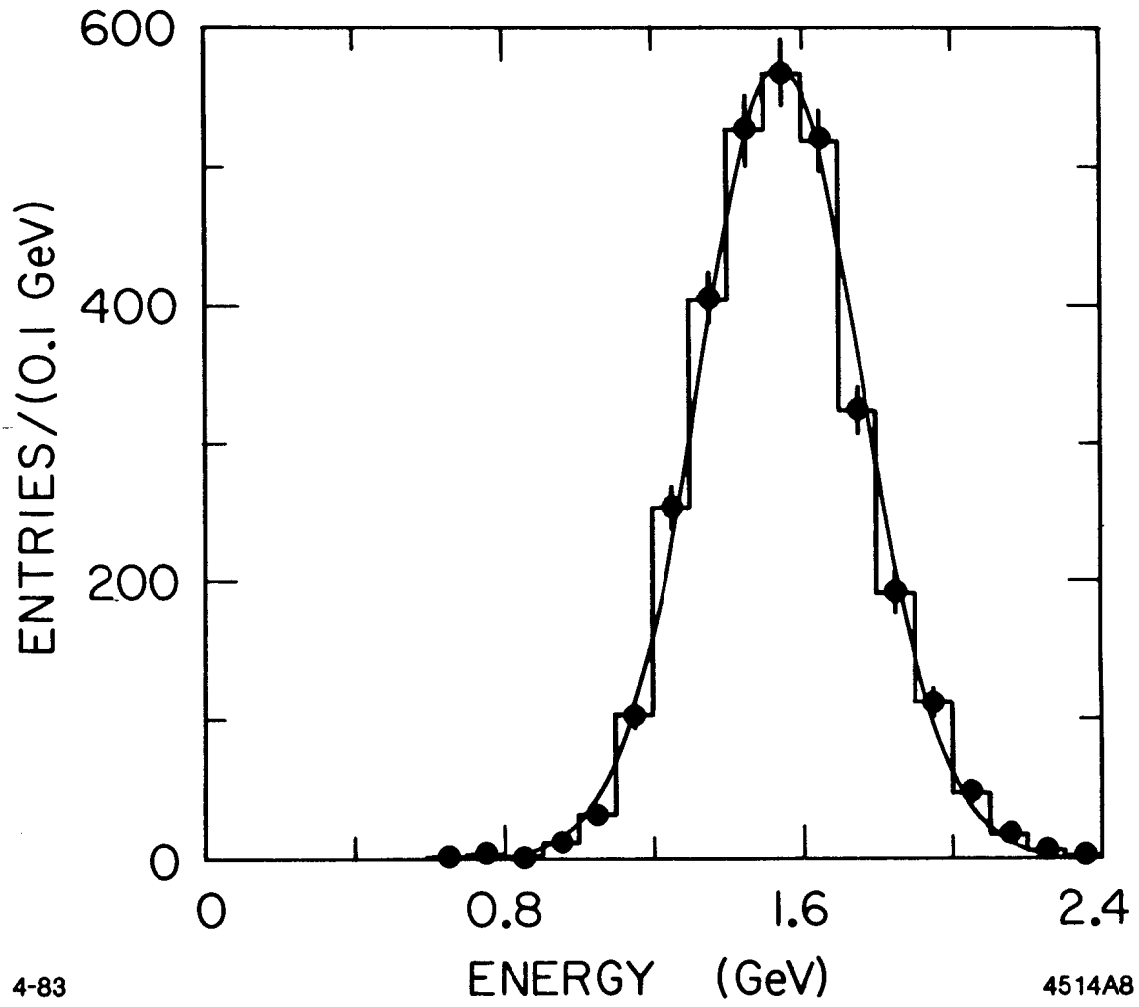

Fig. 10

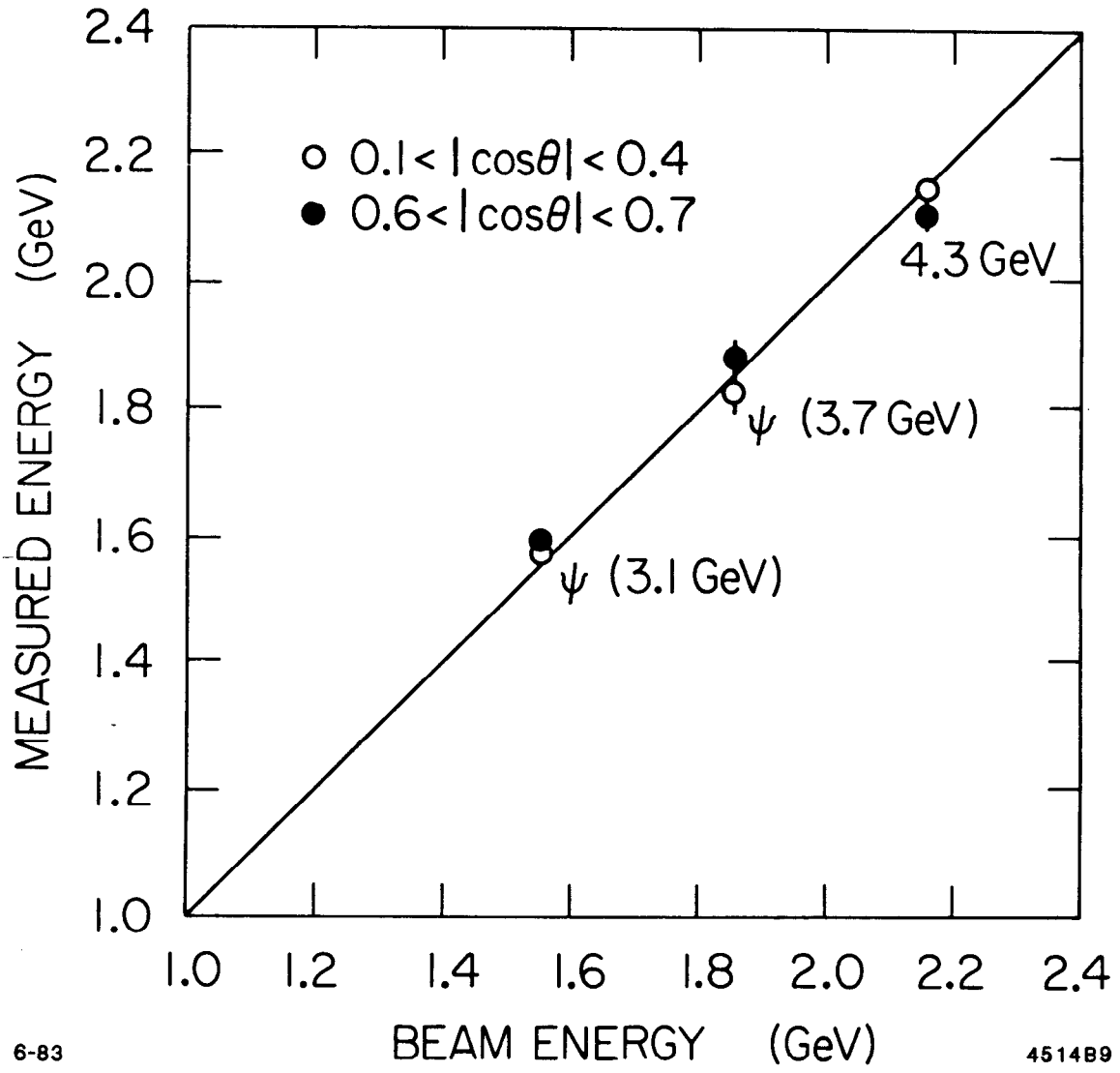
2.4
2.2
2.0
1.8
1.6
1.4
1.2
1.0
MEASURED ENERGY (GeV)
○ 0.1< |cosθ| < 0.4
● 0.6< |cosθ| < 0.7
4.3 GeV
ψ (3.7 GeV)
ψ (3.1 GeV)
1.0 1.2 1.4 1.6 1.8 2.0 2.2 2.4
BEAM ENERGY (GeV)
6-83
4514B9

Fig. 11

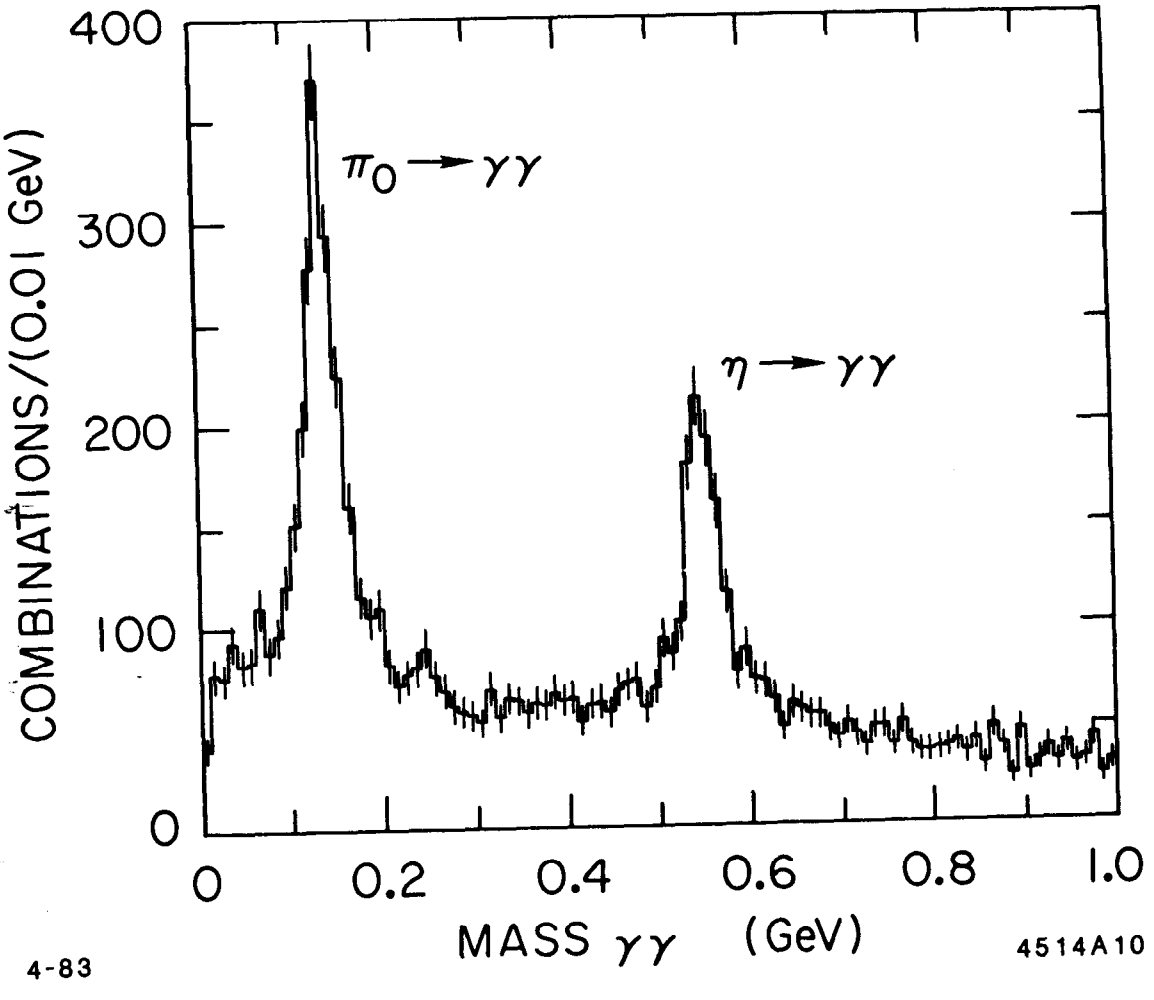
400
300
200
100
0
COMBINATIONS/(0.01 GeV)
$\pi_0 \rightarrow \gamma\gamma$
$\eta \rightarrow \gamma\gamma$
0
0.2
0.4
0.6
0.8
1.0
MASS $\gamma\gamma$ (GeV)
4-83
4514A10

Fig. 12